Frequency Response Function Identification from Incomplete Data
A Wavelet-based Approach

Dirkx, Nic; Tiels, Koen; Oomen, Tom

DOI
10.1016/j.ifacol.2022.11.222

Publication date
2022

Document Version
Final published version

Published in
IFAC-PapersOnline

Available online at www.sciencedirect.com

ScienceDirect

IFAC Papers Online CONFERENCE PAPER ARCHIVE

IFAC PapersOnLine 55-37 (2022) 439–444

Frequency Response Function Identification from Incomplete Data: A Wavelet-based Approach ⋆

Nic Dirkx [*,**] **Koen Tiels** [**] **Tom Oomen** [**,***]

[*] *ASML Research Mechatronics & Control, Veldhoven, The Netherlands*
[**] *Eindhoven University of Technology, Department of Mechanical Engineering, Control Systems Technology, Eindhoven, The Netherlands*
[***] *Delft Center for Systems and Control, Delft University of Technology, Delft, The Netherlands*

Abstract: Frequency Response Function (FRF) identification plays a crucial role in the design, the control, and the analysis of complex dynamical systems, including thermal and motion systems. Especially for applications that require long measurements, missing data samples, e.g., due to interruptions in the data transmission or sensor failure, often occur. The aim of this paper is to accurately identify nonparametric FRF models of periodically excited systems from noisy output measurements with missing samples. The presented method employs a wavelet-based transformation to address the identification problem in the time-frequency plane. A simulation example confirms that the developed techniques produce accurate estimates, even when many samples are missing.

Keywords: Frequency domain identification, non-parametric methods, missing data, transient estimation, linear systems

1. INTRODUCTION

Non-parametric Frequency Response Function (FRF) identification is of key importance in identifying complex systems. FRF identification is considered a fast and inexpensive approach to acquire thorough insight into the system dynamics, while requiring only mild assumptions on the actual system (Ljung et al., 1987).

Dealing with leakage errors, arising from the time-frequency domain transformation of finite-length data records, plays an important role in non-parametric identification. Among different non-parametric FRF identification techniques, the Local Polynomial Method (LPM) (Schoukens et al., 2009; Pintelon et al., 2010) has proven particularly successful in many applications. This method exploits the observation that leakage errors originate from a transient phenomenon, which has smooth frequency characteristics that depend on the system dynamics.

In many practical situations, measurements cannot be performed without interruptions, leading to missing samples in the data record. Missing samples may also be due to sensor or communication link failure (Kar and Moura, 2009). Locally missing samples in the time-domain result in a global and non-smooth perturbation in the frequency domain (Ugryumova et al., 2014), which complicates the use of standard identification algorithms.

Various non-parametric identification methods have been developed to handle the missing samples problem. In Barbé et al. (2012), missing samples are handled by estimating an additional transient for each data gap. A similar strategy is pursued in Schoukens et al. (2012) within an extended LPM framework. The methods become infeasible when the number of data gaps is large.

Different approaches have been developed that aim at estimating reconstructing the missing samples. In Stoica et al. (2009), the missing samples are recovered via a nonparametric iterative spectrum estimation scheme, but system dynamics are not considered. In Ugryumova et al. (2014), the LPM is extended by estimating the missing time-domain samples along with the frequency-domain system and transient parameters. The resulting estimation problem is large-dimensional, especially for many missing samples. In addition, due to the time-frequency domain transform, estimation errors in the locally missing samples result in global errors in the frequency-domain.

Another line of research has focussed on time-dependent frequency analysis of non-stationary signals. In particular, the wavelet transform is widely used in, e.g., signal processing, finite-element methods and image compression (Daubechies, 1990), but is not applied for FRF identification from incomplete data.

Although various techniques for identification from incomplete data exist, at present accurate FRF identification is hampered by a lack of tractable methods that can deal with a large number of missing samples. The aim of this paper is to develop an FRF identification algorithm for periodically excited systems that is applicable to data records with many missing samples.

The main contributions of this paper are:

1. An algorithm that exploits the wavelet transform in a LPM framework for the FRF estimation of linear time-invariant (LTI) systems from incomplete data,
2. an analysis of bias and variance errors,
3. a verification of the method onto a simulation model.

Notations Operations $X = \mathcal{F}x$ and $x = \mathcal{H}X$ denote the Discrete Fourier Transform (DFT) of x and the inverse DFT (IDFT) of X, where $\mathcal{F}$ and $\mathcal{H}$ denote the DFT and IDFT matrices (Rao and Yip, 2018, Ch. 2), respectively. Operator $\odot$ denotes the element-wise product.

⋆ This work was supported by the Research Programme VIDI under Project 15698, partly financed by the NWO.

10.1016/j.ifacol.2022.11.222

2. PROBLEM FORMULATION

2.1 Missing samples identification problem

Consider the input-output relation in the frequency-domain:

$$Y(k) = G(\Omega_k)U(k) + T(\Omega_k) + N_Y(k). \tag{1}$$

Herein, $U \in \mathbb{C}^{NP}$ is the DFT of the N-periodic input signal u, for a number of $P \geq 2$ periods with sample length N. $Y \in \mathbb{C}^{NP}$ is the DFT of the true output signal y obtained from time-domain measurements without missing samples. Furthermore, $G(\Omega_k)$ is the FRF of the true to-be-identified LTI system, at the discrete frequency $\Omega_k = e^{-1i\cdot 2\pi k/NP}$, with $k = 0, \dots NP-1$ the discrete frequency bin. In this paper, the focus is on single-input single-output (SISO) systems, but the presented techniques can also be applied to multiple-inputs multiple-ouputs (MIMO) systems. Term T in (1) is the transient due to the difference between the initial and final conditions of the data (Pintelon et al., 2010). Term $N_Y \in \mathbb{C}^{NP}$ is the DFT of the measurement noise. N_Y is assumed to be circularly complex distributed, zero-mean, with variance λ (Pintelon and Schoukens, 2012, Ch. 14).

Suppose that the output y is measured with interruptions, causing a number of n_m missing samples in its measurement y^m. The measurement is expressed as $y^m = \text{diag}(w)y,\ w \in \mathbb{N}^{NP}$, where

$$w[n] = \begin{cases} 1 \text{ if the } n\text{-th sample is available} \\ 0 \text{ if the } n\text{-th sample is missing} \end{cases}.$$

The DFT of y^m is expressed as $Y^m = \mathcal{T}^m Y$, where

$$\mathcal{T}^m = \mathcal{F}\text{diag}(w)\mathcal{H}. \tag{2}$$

The presence of missing samples significantly complicates the identification of G. Particularly, since $\mathcal{T}^m$ is a full matrix, all frequency lines in Y^m contain data of all the missing samples. So, the locally missing samples in the time-domain have a global impact in the frequency-domain. Consequently, traditional frequency-domain methods that rely on the frequency-separation principle (van Zundert and Oomen, 2019), such as Emperical Transfer Function Estimate (ETFE) method, and the LPM (Pintelon and Schoukens, 2012) can no longer be used.

In this paper, a method is presented for the non-parametric FRF identification of G from incomplete measurements.

2.2 Key idea: wavelet-based estimator

The main limitation in traditional frequency-domain identification methods originates from the fact that the DFT is a global transform, which makes it unsuitable for analysis of signals that exhibit local time-domain phenomena such as missing samples.

The key idea of the identification method presented in this paper is to employ a local wavelet-based transform (Daubechies, 1990) rather than the global DFT transform. In contrast to the DFT, the wavelet-based transform provides time-localized frequency information, enabling two-dimensional analysis in the time-frequency plane. The rationale in view of the missing samples problem is that this allows for FRF identification in the frequency dimension, while the time-domain perturbation of the missing samples can be isolated in the time dimension.

In the next section, concepts of wavelet-based transformation to the time-frequency plane are introduced, which are exploited in the formulation of a wavelet-based estimator in Section 4.

3. MISSING SAMPLES IN TIME-FREQUENCY

3.1 Wavelet-based transformation

The key step in isolating the time-domain perturbation of the missing samples from the frequency-domain characteristics of G and T in (1) is the transformation of the data y^m to the time-frequency plane. This is achieved via convolution with a set of short-time oscillations with frequency f_j, referred to as the wavelet functions $\psi_j,\ j = 1, \dots, n_\psi$.

Definition 1. Consider a signal $y^m \in \mathbb{R}^{NP}$ with DFT Y^m and let $\psi_j \in \mathbb{C}^{NP}$ denote the j-th wavelet function with DFT Ψ_j. Let y^m_{NP} be the NP-periodic extension of y^m,

$$y^m_{NP}[n] = y^m[n - \lfloor n/(NP) \rfloor NP], \quad n \in \mathbb{N}. \tag{3}$$

The circular convolution $z^m_j \in \mathbb{C}^{NP}$ of the signal y^m with the wavelet ψ_j at samples $n = 0, \dots, NP-1$ is defined as

$$z^m_j[n] := \{y^m_{NP} \circledast \psi_j\}[n] := \frac{1}{\sqrt{NP}} \sum_{m=0}^{NP-1} \psi_j[m] \cdot y^m_{NP}[n-m]. \tag{4}$$

The convolution (4) is also expressed as the frequency-domain windowing operation

$$z^m_j = \mathcal{H}(\Psi_j \odot Y^m). \tag{5}$$

Expression (5) shows that Ψ_j acts as frequency-domain windowing function onto the data Y. The transform z_j reflects the evolution over time of the selected frequency components within the local window, thus providing both time- and frequency-localized information.

Missing samples in y^m affect the transform z^m_j. The key idea is to select a suitable wavelet function such that this effect is local. This is considered next.

3.2 Wavelet selection

The aim of the wavelet-based transformation in Def. 1 is to obtain a time- and frequency-domain localized representation of the data y^m, that enables isolating the effect of the missing samples. As implied by Heisenberg-Gabor uncertainty principle, see e.g. Gröchenig (2001), however, there exist fundamental limitations to the accuracy that can simultaneously be achieved in both the domains. The selection of a wavelet therefore involves a trade-off, and its choice is typically specific to the problem at hand.

In this paper, the following class of wavelets is considered.

Definition 2. Let f_j denote a center frequency, $\Delta_f \in \{\mathbb{R} : 1/(\Delta_f T_s) \in \mathbb{N}\}$ a design variable. Then, the wavelet $\psi^{[p]}_j \in \mathbb{C}^{NP}$ is defined as

$$\psi^{[p]}_j[m] = h^{[p]}[m] \cdot e^{1i\cdot 2\pi f_j T_s m}, \quad m = 0, \dots, NP-1.$$

where $h^{[p]} = \sqrt{NP}^{p-1}(\Delta_f T_s)^p \mathcal{H}(\mathcal{F}h)^p$, and $h \in \mathbb{N}^{NP}$ is given by $h[m] = \begin{cases} 1 \text{ if } m \leq 1/(\Delta_f T_s) \\ 0 \text{ otherwise} \end{cases}$. The exponent $p \in \mathbb{N}$ denotes the element-wise exponent.

The following properties apply:

a) $\Psi^{[p]}_j$ equals 1 at the center frequency f_j,

b) $\Psi^{[p]}_j$ is zero at frequencies $f_j \pm \alpha\Delta_f,\ \forall \alpha \in \mathbb{N}$,

c) $|\Psi^{[p]}_j| < |\Psi^{[p+1]}_j|$ at all frequencies except at $f_j \pm \alpha\Delta_f$,

d) $\psi_j^{[p]} := \mathcal{H}(\Psi_j^{[p]})$ *has finite time-domain support of length* $l_\psi = p/(\Delta_f T_s)$*, i.e.,* $\psi_j^{[p]}[n] = 0$ *for* $n > l_\psi$.

Remark 1. Transform (4) for $\psi_j^{[p]}$ as defined in Def. 2 can also be expressed in terms of the discrete-time Short-Time Fourier Transform (Daubechies, 1990).

An example of a wavelet $\Psi_j^{[2]}$ for $j = 1, 2$ and $f_1 = 1$[Hz], $f_2 = 2$[Hz] is shown in Fig. 1, where $N = 500, P = 1, T_s = 0.02[s], \Delta_f = 0.5$. The wavelet enables extracting local frequency-information around f_j within a local time-window of l_ψ samples, see properties a) and d) in Def. 2. Increasing parameter p improves the frequency-domain localization accuracy, at the cost of time-domain localization accuracy, see properties c) and d), respectively.
A crucial property of the wavelets in Def. 2 is their compact time-domain support, see property d). This enables isolating the samples v in $z_j^m[v]$ that are not affected by the missing samples in y^m. Precisely, these samples are given by $v \in \mathcal{V}$ where $\mathcal{V} = \bigcap_{i=1}^{n_m} \mathcal{V}_i$, and

$$\begin{aligned}\mathcal{V}_i = &\big\{v \in \mathbb{N} : \max(w_m[i] - NP + l_\psi, 0) < v < w_m[i] \\ &\text{or } \min(w_m[i] + l_\psi, NP) \le v \le NP\big\},\end{aligned} \tag{6}$$

with $w_m \in \mathbb{N}^{n_m}$ the indices of the missing samples in y^m. The wavelets are applied to construct the time-frequency plane representation in the next section.

3.3 Missing samples in the time-frequency plane

The transformation of incomplete data y^m to the time-frequency domain is illustrated in the following example.

Example 1. Consider a noiseless measurement y^m of size $N = 500$ of the output of a system G, with sampling time $T_s = 0.02$[s]. Samples $220, \dots, 260$ are missing. The system is excited at frequencies $1, \dots, f_{nyq} - 1$Hz, with Nyquist frequency $f_{nyq} = 1/(2T_s)$Hz. A set of wavelets $\psi_j^{[2]}$ with $f_j = 1, \dots, f_{nyq} - 1$, and $\Delta_f = 0.5$ is selected according to Def. 2. The result of wavelet convolution is illustrated in Fig. 2 and explained in its caption.

The main result of the representation as shown in Fig. 2(b) is that $z_j^m[v]$, $v \in \mathcal{V}$, provides unperturbed information of the system G and the transient T in (1). In the next section, the estimator is presented that enables accurate identification of these two individual components.

4. WAVELET-BASED LPM

In this section, the wavelet-based algorithm is presented for accurate FRF identification from incomplete measurements. The method extends the existing the frequency-domain LPM (Pintelon et al., 2011) to an estimator in the time-frequency plane. A recapitulation of the traditional LPM approach is presented first.

4.1 Traditional LPM and its limitations

The LPM (Pintelon et al., 2011) is an effective method for FRF identification in case of complete data. This section recapitulates the traditional LPM for N-periodic input signals u, for $P \ge 2$ periods, and without missing samples. Consider input-output relation (1). For periodic excitations $u \in \mathbb{R}^{NP}$, the DFT $U \in \mathbb{C}^{NP}$ contains energy

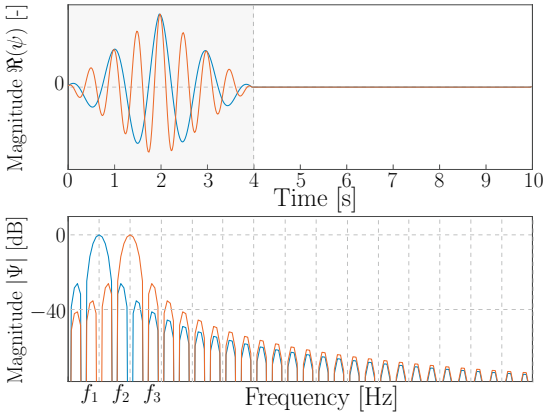

Fig. 1. Wavelets $\psi_j^{[2]}$ in the time- (*top*) and frequency-domain (*bottom*), for $j = 1, 2$. The wavelets extract frequency-information around the frequencies f_1, f_2, respectively, within the finite time-span of the wavelet, indicated by the grey box.

only at the excited frequency (EF) lines γkP with $k = 0, \dots, \lfloor N/\gamma \rfloor - 1$, and $\gamma \in \mathbb{N}$ a user-defined parameter that controls the sparsity of the excitation grid. As such, the system response $G(\Omega_k)U(k)$ is zero at the non-excited frequencies (NEF) lines $\gamma kP + q$ with $q = 1, 2, \dots, \gamma P - 1$, and thus the output (1) at the NEF lines becomes

$$Y(\gamma kP + q) = T(\Omega_{\gamma kP+q}) + N_Y(\gamma kP + q). \tag{7}$$

The transient term is a rational function of the frequency and can be locally approximated by low-order polynomials,

$$T(\Omega_{\gamma kP+q}) = T(\Omega_{\gamma kP}) + \sum_{s=1}^{R} t_s(\gamma k) q^s + \mathcal{O}(q), \tag{8}$$

where $\mathcal{O}(q) = (1/\sqrt{NP})\mathcal{O}\left((q/NP)^{R+1}\right)$ is the remainder of an $(R+1)$-th order Taylor series expansion around $T(\Omega_{\gamma kP})$, see Pintelon et al. (2010). Similarly, at the EF lines, the output (1) is given by

$$Y(\gamma kP) = G(\Omega_{\gamma kP})U(\gamma kP) + T(\Omega_{\gamma kP}) + N_y(\gamma kP). \tag{9}$$

The $R+2$ unknown plant and transient parameters around the excited frequency kP are collected in

$$\Theta_{\gamma k} = \left[\, G(\Omega_{\gamma kP})\ T(\Omega_{\gamma kP})\ t_1(\gamma k)\ \dots\ t_R(\gamma k) \,\right]^T, \tag{10}$$

and are estimated from the $n_r = 2(\gamma P - 1) + 1$ frequency lines around frequency γkP. Choosing $n_r > R + 2$, the estimates are solved from the linear least squares minimization problem,

$$\hat{\Theta}_{\gamma k} = \underset{\Theta_{\gamma k} \in \mathbb{C}^{R+2}}{\arg\min} \left\| Y(\gamma kP + r) - K_{\gamma k}(r)\Theta_{\gamma k} \right\|_2^2, \tag{11}$$

where $r = [-\gamma P + 1, -\gamma P + 2, \dots, \gamma P - 1]^T$, and

$$K_{\gamma k}(r) = \left[\, U(\gamma kP + r)\ r^0\ r^1\ \dots\ r^R \,\right]. \tag{12}$$

Asymmetric windows may be chosen close to the boundaries, see (Pintelon et al., 2010).
The LPM (11) hinges on the principle of frequency separation and local smoothness in the frequency-domain. When missing samples are present, these properties no longer apply. The method presented in this paper aims at recovering these properties.

4.2 Wavelet-based LPM estimator

This section formulates the wavelet-based LPM estimator that extends upon the traditional LPM method (11) for the accurate identification in the presence of missing samples. The extension is twofold. First, the local estimation

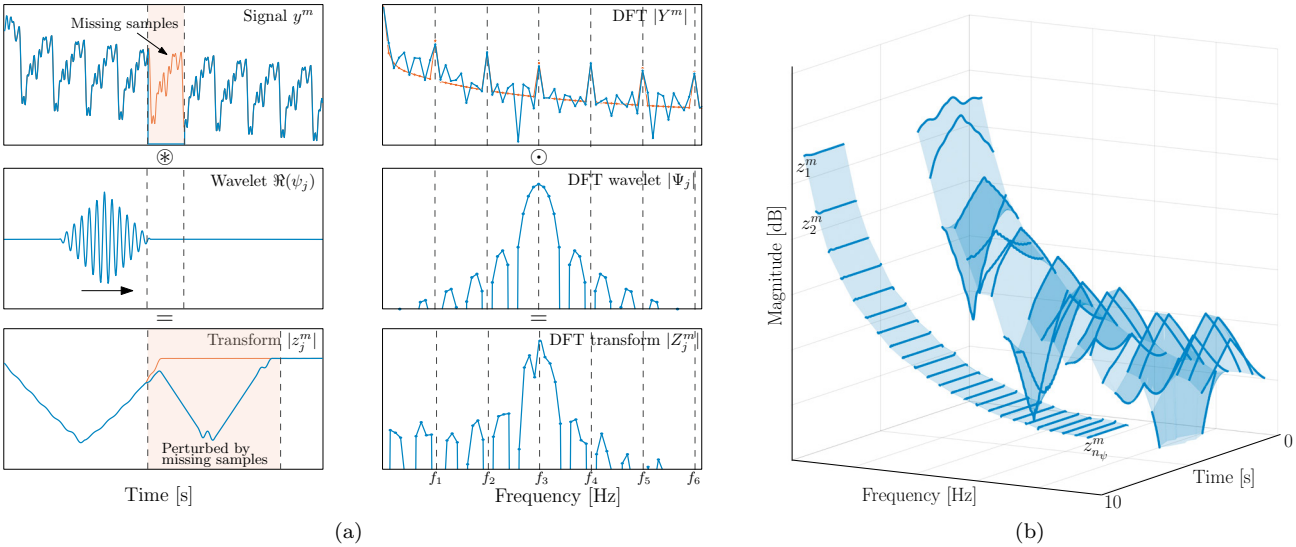

Fig. 2. (a) Wavelet-based convolution of a periodically extended signal y_{NP}^m with a wavelet ψ_j with center frequency f_3, represented in the time-domain (left column) and its frequency-domain counterpart (right column).
Left top: Signal y^m (–) with locally missing samples (–). *Left center:* The convolution is visualized as a translation over time of the wavelet ψ_j with respect to the signal , see (4). *Left bottom:* Transforms $z_j^m = \{y_{NP}^m \circledast \psi_j\}$ (–), and $z_j = \{y_{NP} \circledast \psi_j\}$ in case of complete data (–). The perturbation due to the missing samples in z_j^m is isolated within the red box, whereas the samples outside provide unperturbed information of the system G and the transient T in (1).
Right top: The DFT Y^m (–) and the DFT Y (- -). Missing samples form a global perturbation in Y^m. *Right center:* The DFT Ψ_j. The energy of the wavelet is approximately localized around the center frequency f_3.*Right bottom:* The DFT Z_j^m has its energy approximately concentrated around the center frequency f_3.
(b) The transforms z_j^m, $j = 1, \dots n_\psi$, in the time-frequency plane. Only the unperturbed samples $v \in \mathcal{V}$, see (6), are displayed.

criteria (11) are combined into a single global estimation criterion, to account for the global effect of the missing samples. Second, a global weighting matrix $\bar{M}$ is introduced that incorporates the wavelet-based transformation. The estimation criterion is formulated as

$$\hat{\bar{\Theta}} = \underset{\bar{\Theta} \in \mathbb{R}^{2n_\Theta}}{\arg\min} \left\| \bar{M}(Y^m - \bar{K}\bar{\Theta}) \right\|_2^2 . \tag{13}$$

Herein, $n_\Theta = n_\psi(R+2)$, and the parameters are given by

$$\bar{\Theta} = \begin{bmatrix} \Re\left(\begin{bmatrix} \Theta_{\gamma\cdot 1}^T & \dots & \Theta_{\gamma n_\psi}^T \end{bmatrix}^T \right) \\ \Im\left(\begin{bmatrix} \Theta_{\gamma\cdot 1}^T & \dots & \Theta_{\gamma n_\psi}^T \end{bmatrix}^T \right) \end{bmatrix} .$$

where $\Theta_{\gamma j}$ is of the form (10). The global regressor $\bar{K}$ is defined as

$$\bar{K} = \begin{bmatrix} 0_{1\times n_\Theta} & 0_{1\times n_\Theta} \\ \tilde{K} & 1i \cdot \tilde{K} \\ 0_{1\times n_\Theta} & 0_{1\times n_\Theta} \\ \mathcal{I}_{n_\Theta}\mathrm{conj}(\tilde{K}) & -1i \cdot \mathcal{I}_{n_\Theta}\mathrm{conj}(\tilde{K}) \end{bmatrix},$$

where $\mathcal{I}_{n_\Theta}$ is an n_Θ-sized exchange matrix, the zero rows in $\bar{K}$ correspond to the zero and Nyquist frequencies, and

$$\tilde{K} = \begin{bmatrix} K_{\gamma\cdot 1}(r) & & \\ & \ddots & \\ & & K_{\gamma n_\psi}(r) \end{bmatrix} . \tag{14}$$

The regressor submatrices $K_{\gamma\cdot j}(r)$ in (14) are of the form (12), yet the local window is selected as $r = [-\lceil 1/2\gamma P - 1 \rceil, -\lceil 1/2\gamma P - 2 \rceil, \dots, \lceil 1/2\gamma P - 2 \rceil, \lceil 1/2\gamma P - 1 \rceil]$.
By choosing the matrix $\bar{M}$ in (13) as $\bar{M} = I$, the solution of the global estimator (13) recovers that of the classical LPM (11), given the same choice of r and R. Hence, (13) forms a generalization of (11). The key point of formulation (13) is that $\bar{M}$ provides the additional freedom to incorporate the time-frequency plane transformation. This is achieved by setting $\bar{M} = \begin{bmatrix} M_1^T & \dots & M_{n_\psi}^T \end{bmatrix}^T$, where

$$M_j = \mathcal{W}\mathcal{H}\mathrm{diag}(\Psi_j), \quad j = 1, \dots, n_\psi. \tag{15}$$

Herein, the wavelets Ψ_j are selected according to Def. 2. Specifically, to obtain a sensible wavelet design, the center frequencies of the wavelets are selected to coincide with the EF lines via $f_j = \gamma j P/(NT_s)$. Additionally, the parameter Δ_f is selected as $\Delta_f = 1/2(f_{j+1} - f_j)$. The rationale of this selection is that, by Def. 2, property a), the wavelet extracts local frequency-information around the j-th EF, while interaction from the other EF lines is eliminated, see property b).
The matrix $\mathcal{W}$ in (15) is a diagonal matrix that selects only the data that are not affected by the missing samples,

$$[\mathcal{W}]_{q,q} = \begin{cases} 1 \text{ if } q \in \mathcal{V} \\ 0 \text{ otherwise} \end{cases}, \quad q = 1, \dots, NP, \tag{16}$$

where $\mathcal{V}$ is defined in (6).

Consider the following result.

Theorem 1. Consider a measurement y^m with missing samples, and its DFT Y^m. Suppose that the contributions due to the remainders $\mathcal{O}$ and measurement noise N_Y in (7) and (8) are zero, such that $Y = \bar{K}\bar{\Theta}$. Then, the solution $\hat{\bar{\Theta}}$ to (13) is exact, i.e., $\hat{\bar{\Theta}} = \bar{\Theta}$, if

i) $\bar{M}\bar{K}$ has full column rank,
ii) $M_j(Y - Y^m) = 0$ for $j = 1, \dots, n_\psi$.

The proof is omitted to conserve space. The underlying mechanism for the result in Thm. 1, is that, by condition ii) the samples of z_j^m, see (5), that are affected by the missing samples in y^m are discarded from the estimation problem. Condition ii) is satisified by (16). Additionally, condition

i) ensures that the remaining data are sufficiently informative to estimate the n_Θ parameters.
The conditions i), ii) for exact identification in the sense of Thm. 1 impose only mild requirements on matrix $\bar{M}$ and hence on the selection of the wavelet function. In the presence of remainders $\mathcal{O}$ and measurement noise N_y, see (8) and (9), however, the wavelet design plays an important role in the trade-off between variance and bias errors. This is analyzed in the next sections.

4.3 Variance

The variance in the parameter estimates is generally a complex nonlinear function of, amongst others, the number and the location of the missing samples and the choice of wavelet. To achieve low-variance estimates, the number of retained samples in z_j^m should ideally be maximized, as is implied by the following result.

Theorem 2. The variance of the estimates $[\hat{\bar{\Theta}}]_q$, $q = 1, \dots n_\Theta$ *is upper-bounded by*

$$\operatorname{var}([\bar{\Theta}]_q) \;\leq\; \bar{\sigma}(\bar{B}) \left[P_\Theta^{-1}\right]_{q,q} \;\leq\; \left[P_\Theta^{-1}\right]_{q,q},$$

where $\bar{B} = \bar{M}^H \bar{M}$ *and* $[P_\Theta^{-1}]_{q,q}$ *is the* $[q,q]$ *entry of the inverse of the information matrix,*

$$P_\Theta = \frac{2}{\lambda} \Re \sum_{i \in \mathcal{V}} \sum_{j=1}^{n_\psi} \left(\mathcal{H}_i \operatorname{diag}(\Psi_j) \bar{K}\right)^H \left(\mathcal{H}_i \operatorname{diag}(\Psi_j) \bar{K}\right),$$

with $\mathcal{H}_i$ *denoting the* i*-th row of* $\mathcal{H}$.

The proof is omitted to conserve space. Thm. 2 gives rise to the formulation of the minimal variance estimator.

Corollary 3. Estimator (13) achieves minimal variance for the wavelet $\Psi_j^{[0]}$, *i.e.,* $\Psi_j^{[0]} = 1_{NP}$. *Its variance is computed by* $\operatorname{var}(\bar{\Theta}_q) = [P_\Theta^{-1}]_{q,q}$ *where,*

$$P_\Theta = \frac{2}{\lambda} \Re \sum_{i \in \mathcal{V}} \left(\mathcal{H}_i \bar{K}\right)^H \left(\mathcal{H}_i \bar{K}\right). \tag{17}$$

Cor. 3 recovers the situation without wavelet function, by which the transform (5) reduces to the IDFT. Indeed, the IDFT has perfect time-domain localization, and hence maximizes the size of $\mathcal{V}$. However, the IDFT does not provide frequency-domain localization, which has negative impact on bias errors. This is analyzed next.

4.4 Bias

Bias in the parameter estimates due to the remainders $\mathcal{O}$ in (8) plays a particularly important role in FRF identification when samples are missing. To see this, suppose that the matrices $\bar{M}, \bar{K}$ are selected such that conditions i), ii) in Thm. 1 hold. Then, when $N_Y = 0$, the parameter estimate is expressed as

$$\hat{\bar{\Theta}} = \bar{\Theta} + \left(\Re\left(\bar{K}^H \bar{B} \bar{K}\right)\right)^{-1} \Re\left(\bar{K}^H \bar{B} \bar{\mathcal{O}}\right), \tag{18}$$

where $\bar{B} := \bar{M}^H \bar{M}$, and $\bar{\mathcal{O}} = \begin{bmatrix} \mathcal{O}_1^T & \dots & \mathcal{O}_{n_\psi}^T \end{bmatrix}^T$. Expression (18) shows that matrix $\bar{B}$, when non-diagonal, introduces global coupling between the local estimates Θ_j, despite the original decoupled (block-diagonal) structure of $\bar{K}$ in (14). Thus, matrix $\bar{B}$ is an indicator of coupling and coupling-induced bias errors in (13). Expressing matrix $\bar{B}$ as

$$\bar{B} = \bar{M}^H \bar{M} = \sum_{j=1}^{n_\psi} \operatorname{diag}(\Psi_j)^H \mathcal{F} \mathcal{W} \mathcal{H} \operatorname{diag}(\Psi_j), \tag{19}$$

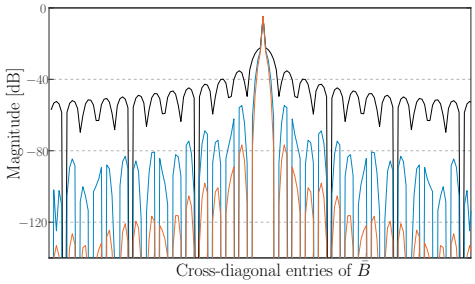

Fig. 3. The cross-diagonal entries of $\bar{B}$ for $p = 0$ (−), $p = 1$ (−), and $p = 2$ (−), as indicator for coupling . The coupling reduces significantly for increasing values of p.

shows that the wavelet functions Ψ_j form the crucial design parameters to shape the matrix $\bar{B}$ and hence to mitigate the bias errors. The following example demonstrates the role of the wavelet in diagonalization of $\bar{B}$.

Example 2. Consider the scenario of Example 1, for wavelets $\psi_j^{[p]}$ for $p = 0, 1, 2$. To visualize the achieved diagonal dominance of the matrix $\bar{B}$, see (19), its cross-diagonal entries are depicted in Fig. 3.

Example 2 and (19) show that achieving (approximate) diagonality of $\bar{B}$ requires wavelet functions with good, or in fact perfect, frequency-domain localization properties. This observation, in conjunction with Cor. 3, indicates that variance minimization and bias minimization require the opposite wavelet functions, which once more illustrates the inherent trade-off in wavelet selection.

5. SIMULATION STUDY

5.1 Simulation setup

The presented techniques applied for the identification of a simulation model G with 2 highly and 2 lightly damped modes, shown in Fig. 6. $P = 10$ periods are measured, with sample length $N = 500$ and sampling time $T_s = 0.02$[s]. The system exhibits a significant transient for the entire duration of the measurement. The output signal contains five data gaps, with in total $n_m = 625$ missing samples. In addition, the output is perturbed by measurement noise with variance $\lambda = 10^{-2}$. The EF lines are chosen at $\gamma k P, k = 1, \dots, 1/(2T_s)$ with sparsity parameter $\gamma = 2$, and the spectral excitation magnitudes are uniformly distributed over the EF lines. The wavelets defined in Def. 2 are selected for the values $p = 0, 1, 2$, giving rise to three different estimators. In all cases, the LPM polynomial order is chosen as $R = 2$.

5.2 Identification results - noiseless case

First, identification in the noiseless case is considered, i.e., $N_Y = 0$. The result of wavelet convolution, the estimated plant, and transient for $\psi_j^{[2]}$ are shown in Fig. 4. The estimate $\hat{G}$ accurately represents G. To analyze the bias, the DFT of the estimated transient is depicted in Fig. 5. Despite the high level of non-smoothness in T^m, the estimated transient $\hat{T}$ accurately matches the smooth transient T. The larger errors around the first resonance are due to the use of low-order ($R = 2$) polynomials. The bias remains localized around the first resonance, which indicates good frequency-localization.

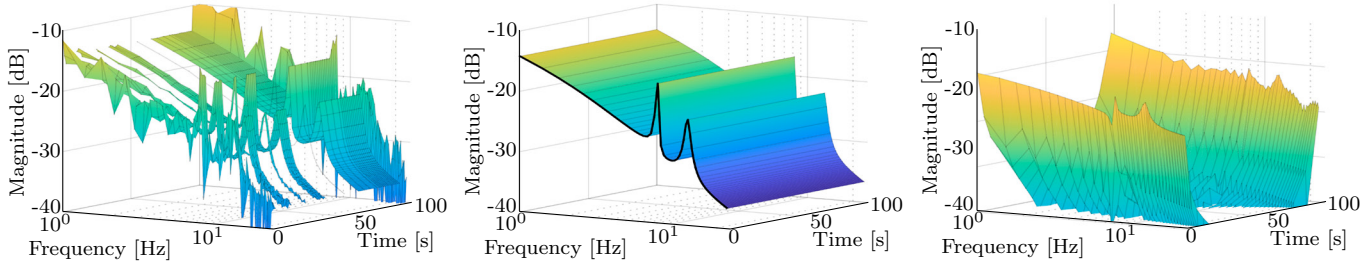

Fig. 4. time-frequency plane results for $\psi_j^{[2]}$. *Left:* The transforms $z_j^m[v],\ j = 1, \ldots, n_\psi$ for samples $v \in \mathcal{V}$. *Center:* Estimate $\hat{G}$ (surface) and FRF of true system G (black). *Right:* Estimate of transient T.

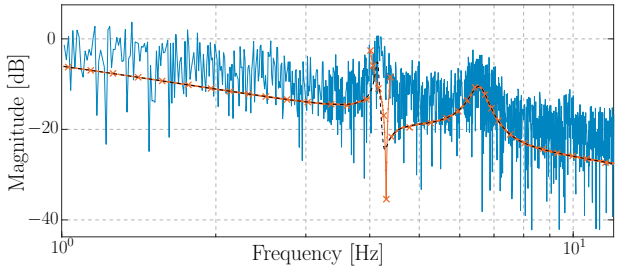

Fig. 5. The non-smooth transient DFT T^m (−), the smooth transient T (−), and the estimate $\hat{T}$ (×−) based on non-smooth data. The estimate accurately represents the true smooth transient.

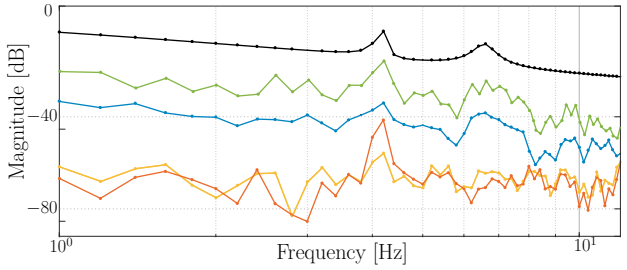

Fig. 6. FRF of true system G (−), and the identification errors for traditional LPM (−), wavelet-based LPM for $p = 0$ (−), $p = 1$ (−), and $p = 2$ (−). Traditional LPM yields large errors. For the wavelet-based estimators, the errors for $p = 0$ are largest due to coupling-induced bias. The errors for $p = 1$ and $p = 2$ are substantially smaller and of comparable magnitude.

5.3 Identification results - with noise

Next, the identification errors in the noisy case of the three estimators and of the traditional LPM are compared in Fig. 6. Traditional LPM achieves poor performance, since it does not explicitly account for missing samples. Among the wavelet-based estimators, the minimal variance estimator ($p = 0$) achieves lowest performance, since its error is heavily affected by coupling-induced bias, recall Section 4.4. This underlines the necessity of using frequency-localized wavelets. This is supported by the errors for $p = 1, 2$, which are significantly smaller despite the increased variance. The estimator with $p = 2$ achieves lowest bias, which is observed from the small error around the first resonance frequency.

6. CONCLUSIONS

The presented method enables accurate FRF identification from data records with many missing samples. This is realized by exploiting a wavelet-based transformation in a LPM framework to achieve joint localization of the missing samples in the time-domain, and of bias errors in the frequency-domain. In contrast to most existing algorithms, the problem-size of the presented method reduces with an increasing number of samples. Simulation results demonstrate good performance. Future work will focus on extending theoretical results and experimental validation.

REFERENCES

Barbé, K., Van Moer, W., Lauwers, L., and Björsell, N. (2012). A simple nonparametric preprocessing technique to correct for nonstationary effects in measured data. *IEEE Trans. Instrum. Meas.*, 61(8), 2085–2094.

Daubechies, I. (1990). The wavelet transform, time-frequency localization and signal analysis. *IEEE Trans. Inf. Theory*, 36(5), 961–1005.

Gröchenig, K. (2001). *Foundations of time-frequency analysis*. Springer Science & Business Media.

Kar, S. and Moura, J.M. (2009). Distributed consensus algorithms in sensor networks: Quantized data and random link failures. *IEEE Trans. Signal. Process.*, 58(3), 1383–1400.

Ljung, L. et al. (1987). *System Identification: Theory for the user*. Prentice-hall, Inc.

Pintelon, R. and Schoukens, J. (2012). *System identification: a frequency domain approach*. John Wiley & Sons.

Pintelon, R., Schoukens, J., Vandersteen, G., and Barbé, K. (2010). Estimation of nonparametric noise and FRF models for multivariable systems—part I: Theory. *Mech. Syst. Signal. Process.*, 24(3), 573–595.

Pintelon, R., Vandersteen, G., Schoukens, J., and Rolain, Y. (2011). Improved (non-) parametric identification of dynamic systems excited by periodic signals—the multivariate case. *Mech. Syst. Signal. Process.*, 25(8), 2892–2922.

Rao, K.R. and Yip, P.C. (2018). *The transform and data compression handbook*. CRC press.

Schoukens, J., Vandersteen, G., Barbé, K., and Pintelon, R. (2009). Nonparametric preprocessing in system identification: a powerful tool. In *2009 Eur. Control Conf. (ECC)*, 1–14. IEEE.

Schoukens, J., Vandersteen, G., Rolain, Y., and Pintelon, R. (2012). Frequency response function measurements using concatenated subrecords with arbitrary length. *IEEE Trans. Instrum. Meas.*, 61(10), 2682–2688.

Stoica, P., Li, J., Ling, J., and Cheng, Y. (2009). Missing data recovery via a nonparametric iterative adaptive approach. In *2009 IEEE International Conference on Acoustics, Speech and Signal Processing*, 3369–3372.

Ugryumova, D., Pintelon, R., and Vandersteen, G. (2014). Frequency response function estimation in the presence of missing output data. *IEEE Trans. Instrum. Meas.*, 64(2), 541–553.

van Zundert, J. and Oomen, T. (2019). Beyond equidistant sampling for performance and cost: A loop-shaping approach applied to a motion system. *Int. J. Robust Nonlinear Control*, 29(2), 408–432.